Prediction of Crushing Stress in Composite Materials

S Goh[#], H Ku[#+] and S L Ang[#]

[#]Faculty of Engineering and Surveying,
University of Southern Queensland, Australia;
[+]Centre of Excellence for Engineered Fibre Composites
University of Southern Queensland, Australia.

Corresponding Author:
Title : Dr.
Name : Harry Siu-lung Ku
Affiliation : Faculty of Engineering and Surveying,
University of Southern Queensland.
Tel. No. : (07) 46 31-2919
Fax. No. : (07) 4631-2526
E-mail : ku@usq.edu.au
Address : Faculty of Engineering and Surveying,
University of Southern Queensland,
West Street, Toowoomba, 4350,
Australia.

Abstract: A simple mathematical model for predicting the crushing stress of composite materials was derived and presented in this paper. The present knowledge of fracture mechanics and strength of materials are used as the basis for the model. The fracture mechanics part of the analysis was based on energy release rate approach; the energy release rate, G, of the proposed model was determined by this approach. This energy release rate was based on the Mode I (opening or tensile mode) failure. As for the strength of materials part analysis, buckling theory was used to determine the critical load of the fibre beams. These two engineering concepts were combined to form the equation for the proposed model. The derived equation is a function of the materials properties, geometric and physical parameters of the composite materials. The calculated stresses from the derived equation were compared with experimental data from technical and research papers. Good agreements shown in the results are encouraging and recommendations for future analysis with different modes of failure were also presented. This paper enables engineering designers to predict crushing stress in composite materials with confidence and makes their work more efficient and reliable.

Keywords: composite materials, crushing stress, fracture mechanics cracking opening angle and buckling theory.

1. Introduction

Composite materials have played an important role in achieving overall performance improvements in advanced structure. However, these benefits are often limited by premature damage in the form of fracture and delamination. Since structures

consisting of composite members are getting larger and more complex, the joining of several structural members is becoming more and more common, and design is more often dictated by the structural joint strength.

Joining by mechanical fasteners is a common technology for assembling structural components in the aerospace and automobile industries. It is well known that fasteners can severely reduce the load bearing capacity of the composite materials by more than fifty percent. Due to anisotropy and inhomogenity of composite materials, the failure and strength of bolted composite joints can be considerably different from the failure and strength of metallic joints. Damage in bolted composite joints can initiate, at an early loading stage, and accumulate inside the composite materials as the load increases. This accumulation and failure mode strongly depend on the material, ply orientation, laminate thickness, joint geometry and loading conditions and so on.

There are three basic joint failure modes related to composite joints: net tension, shear out and bearing. Joint failures with the first two modes are catastrophic resulting from excessive tensile and shear stresses. However bearing damage is progressive and is related to compressive failure. The objective of this project is to model the bearing failure of the composite joint with that of progressive crushing. To model the crushing stress model, two engineering concepts were used, fracture mechanics and strength of the materials. The energy release rate approach of linear elastic fracture mechanics was used to develop the energy release rate (G) of the model. Using the buckling

theory of mechanics of materials, the critical load (P_{cr}) can be found for the fibre strand.

Combining these two concepts, the crushing stress therefore can be derived. The derived equation should be a function of the following properties or parameters:

G	-	Energy release rate of the laminate
E	-	Modulus of the laminate in the transverse direction
θ	-	Crack opening angle in degree
h	-	Thickness of the composite
a	-	Crack length

Therefore in a generalized mathematical form, the crushing stress is

$$\sigma_c = f(G, E, \theta, h, a)$$

Figure 1 illustrates the general representation of the model

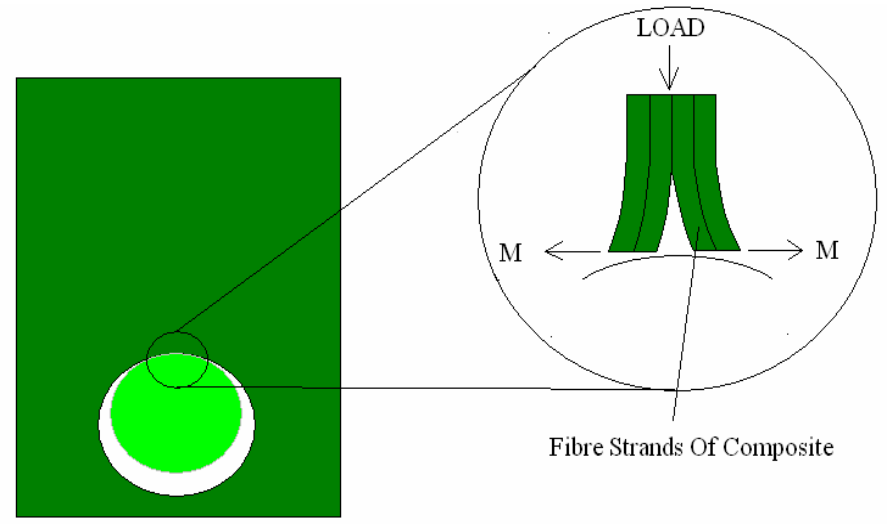

Figure 1: General Model Representation

2. Previous Works on Crushing Behaviour and Specific Energy Absorption

Because of their inherent flexibility in their design for improved materials properties, composite materials have wide applications in automobile and aerospace industries. However their failure mechanism is highly complicated and rather difficult to analyze. Some of previous works are mentioned briefly in the coming paragraphs.

Farley and Jones studied the effect of crushing speed on the energy absorbing characteristic of kelvar/epoxy and graphite/epoxy tubes and found that for graphite/epoxy tubes with [0±θ] fibre orientation, the specific energy did not vary with the crushing speed but the reverse were true for [±θ] fibre orientation [1]. In kelvar/epoxy tubes, however, the energy absorption capacity increases with speed in all cases considered.

Further studies were carried out by Farley and Jones to find the specific energy for different ply orientation and geometries of kelvar/epoxy and graphite/epoxy tubes [2]. A commercially available non-linear FEM program (EAL – Engineering Analysis Language) was used for this purpose. For the kelvar/epoxy tubes the program predicted an energy absorption capability slightly increase between θ=15˚ and 45˚ and decreases between θ=45˚ and 75˚. This finding is 25 percent higher than experimental results. For the graphite/epoxy tubes, the predicted energy absorption capability is highest at θ=15˚ and decreases in a near linear manner as θ increases. The predicted value is 28 percent higher than experimental values at θ=15˚ whereas at θ=75˚ the predicted values is 22 percent of the experimental value. The agreement between analytical and experimental suggests that the important phenomena of the crushing process have been included in the model.

Tao et al. presented a simplified model to predict the average crushing stress of composite rods by considering various factors that influence their energy absorption [3]. His model showed that the energy absorption properties of unidirectional fibre composite rods specimens were dependent on the fibre volume fraction and properties of the fibres and matrix, such as the fibre diameter, the matrix compressive strength and the bonding between the fibres and matrix. The volume specific energy absorption was found to increase with fibre content, fibre diameter, matrix yield strength and crush rate.

Hull summarized that the crush geometry and force-displacement response was interrelated and that the wide range of materials and testing variables that affected the crushing behaviour can be accounted for on this basis [4]. The fracture mode of composite tubes made from brittle fibres and resins occurs by fragmentation or splaying, singly or in combination. These two different modes of fracture involved two completely different types of mechanisms. By changing the fibre distribution it was possible to change the micromechanisms of crush and hence control the load bearing capacity of the tubes during progressive crushing. For some fibre arrangement, the crushing speed had relatively little effect on the crushing behaviour and no change in crushing mode was observed. However, for some fibre arrangements, a small change in the crushing speed can caused a significant change in the crushing mode. Variables such as geometry and dimension can also affect the crush mode. It had been reported that for a same material with different values of Diameter (D), thickness (t) and D/t ratio, the difference in the specific crushing stress was very significant.

Hamada et al. carried out compression tests to determine the effects of glass surface treatment on the crushing behaviour [5]. The materials used were glass cloth/epoxy composite tubes with different glass/matrix surface treatment. Two kinds of surface treatment were used: acryl silane and amino silane coupling agents. The fracture mode of amino silane treated tubes was by splaying, whereas in the acryl treated tubes the fragmentation mode of crushing was observed. The axial crushing performance of the amino treated tubes is approximately 25 percent greater than the acrly treated ones.

Hamada et al. has demonstrated that a unifying theme is the influence of these many factors on the crush zone morphology, which, in turn, controls the ability of the crushing element to bear the load during crushing [6]. The specific energy absorption, E_S, is defined as $E_S = \sigma_{mean} K/\rho$

where σ_{mean} is the mean crush stress, ρ is the density and K is the efficiency factor relating to the way that crush debris is dispersed.

Experiments have been carried out on the influence of fibre architecture and matrix properties on energy absorption in the carbon fibre/polymer-matrix composite tubes. The materials used were carbon/epoxy and carbon/PEEK composite tubes. The most remarkable feature of these results is the very high specific energy absorption (180 KJ Kg^{-1}) obtained in the 0˚ carbon/PEEK tubes. In contrast, the 0˚ carbon/epoxy tubes failed at low loads with extensive cracking parallel to the fibres. The mode 1 fracture toughness (G_{Ic}) obtained for the carbon/PEEK was in the range 1560-2400 J m^{-2} and 120-180 J m^{-2} for the carbon/epoxy, using DCB (double cantilever bean) method. The compressive strength obtained on the 0˚ tubes show that, provided buckling is

avoided, very high values (530 MPa for carbon/PEEK and more than 490 MPa for carbon/epoxy) can be achieved.

Hamada et al. carried out further studies on the carbon fibre/PEEK to identify the factors, which contribute to the superior energy absorption performance of these tubes. The carbon fibre/PEEK tubes used in this study were the APC-2/AS4 with a volume fraction of 0.61 [7]. During axial compression loading of carbon/PEEK tubes, three steps sequentially take place prior to the establishment of a stable crush zone. First, the tube wall fractured and was followed by the longitudinal cracking of the tube wall. Lastly, longitudinal cracks cease to grow and the tube wall splays into internal and external fronds. These longitudinal cracks were observed to be ≈ 0.5 mm long, for carbon/PEEK, as compared to the 8 mm long cracks reported for carbon/epoxy tubes. During the steady-state progressive crushing, there were two main fracture processes, i.e., splitting of fronds into thin beams and fracture of fibres. It was found that the superior performance of the carbon/PEEK tubes is attributed to the higher fracture toughness of the composite materials, splitting of strands and the large number of fibre of fractures.

Gupta et al. studied the variation of the tube crush zone length (length crushed in a single cycle) with variation in its D/t ratio [8]. Analysis was carried out to find the average crush stress for both empty and foam filled FRP tubes of different ratios under axial compression. The expressions are obtained by considering various energy terms involved in the crushing process. The average crushing stress obtained by the derived expressions are compared with experimental results and results show that

increase in D/t ratio increases the average crushing stress and the same was observed in the experimental values.

Dubey and Vizzini compared the energy absorption of composite plates and tubes [9]. All plate and tube specimens were manufactured from AS4/3501-6 graphite/epoxy with the same lay-up and thickness, thus providing a common laminate for comparison. Results indicated that specimen geometry affects specimen stability and therefore the failure modes exhibited by the specimen during crushing. Similar failure modes were observed in the tube and flat-plate specimens with the flat plates absorbing 12 percent less energy per unit mass. These can be attributed to the difference in the effective D/t ratio.

3. Previous Works on Strain Energy Release Rate and Interlaminar Fracture Toughness of Composite Materials

Analysis of the strain energy rate of a given geometry and loading is vital for the prediction of delamination or interlaminar flaw growth. Wang overviewed the fracture mechanics approach as applied to composite materials, using the strain energy release rate as a crack extension criterion [10]. The strain energy release rate using the crack closure method was calculated and prediction based on the critical strain energy release rate was also made [10 – 11].

O' Brien and O' Brien et al. derived a simple closed form equation for the strain energy rate, *G*, associated with edge delamination growth in unnotched laminates by using the laminated plate theory [12 – 13]. Results of *G* using his equation were in

good agreement with finite element analysis. His findings led to the use of the edge delamination test as a proposed standard test for fracture toughness.

The most commonly used test for interlaminar fracture toughness characterization in mode I is the DCB (double cantilever beam) test. Two basic configurations were used, the constant width and the tapered width. Strain energy release rate obtained by the WTDCB (tapered width) is independent of crack length, *a*, the crack grows under a constant load [14]. Using the DCB, Ramkumar and Whitcomb characterized the interlaminar fracture toughness of the T300/5208 composite laminates [15]. Two lay-up configurations were used and the G between the two lay-up was small.

4. Linear Elastics Fracture Mechanics (LEFM)

The elastics fracture mechanics deals with the prediction of fracture strength of relatively brittle materials. The linear elastic materials are assumed to be isotropic and contain pre-existing cracks. In the analysis of the problem in this project, the energy release rate approach of the linear elastics fracture mechanics was used.

The first successful analysis of the energy release rate method was done by Griffith in 1920. His reasoning was based on the hypothesis that the free energy of a cracked body and the applied force should not increase during crack extension. This hypothesis allows the estimation of the theoretical strength and also gives the correct relationship between fracture strength and defect size. The general equation of the Griffith's energy approach was given as [16]:

$$\frac{d}{da}\left(F - U_a\right) \geq \frac{dU_\gamma}{da} \qquad \text{..... (1)}$$

O' Brien pointed out by another researcher that Griffith's type energy balance must be between

(1) the stored strain energy and

(2) the surface energy plus the work done in plastic deformation

and defined a material property G as the total energy absorbed during cracking per unit increase in crack length and per unit thickness [12]. This material property G is called the "crack driving force" or "energy release rate".

Since the right hand side of Griffith's equation is the total energy absorbed during cracking and G as defined by O' Brien is the total energy absorbed during cracking, therefore Griffith's equation can be re-written as

$$\mathrm{G} = \frac{d}{da}\left(F - U_a\right) \qquad \text{..... (2)}$$

In this project, the crack between the piles was modeled as a double cantilever beam (DCB) specimen as shown in Figure 2. For a DCB specimen the force F is equal Pv and U_a is equal to half of the force. Therefore Equation (2) can be written as

$$G = \frac{d}{da}\left(F - U_a\right) = \frac{1}{b}\left(P\frac{dv}{da} - \frac{dU_a}{da}\right)$$

$$= \frac{1}{b}\left(P\frac{dv}{da} - \frac{dPv}{2da}\right) \qquad \text{..... (3)}$$

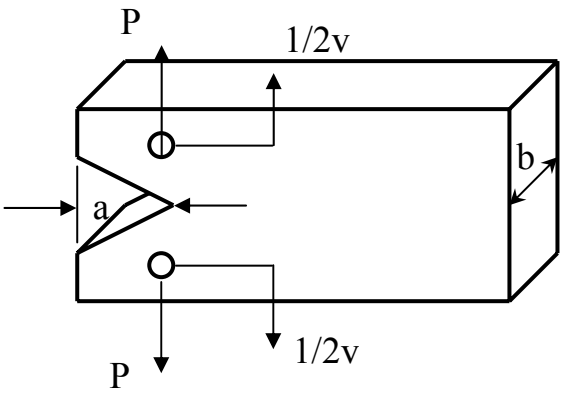

Figure 2: A typical DCB specimen configuration

By introducing the compliance of the body, C, which is the inverse of the stiffness,

i.e. $C = \frac{v}{P}$

the above equation (3) becomes

$$G = \frac{P^2}{2b}\left(\frac{dC}{da}\right) \qquad \text{..... (4)}$$

for a Mode I, double cantilever beam (DCB)

$$\frac{dC}{da} = \frac{24a^2}{Ebh^3} \qquad \text{.....(5)}$$

By substituting (5) into (4), $G = \frac{P^2}{2b}\ \frac{24a^2}{Ebh^3}$

$$G = \frac{12P^2a^2}{Eb^2h^3} \qquad \text{..... (6)}$$

4.1 Relationship of G and the Stress Intensity Factor K_1

For a plane stress condition,

$$\frac{dU_a}{da} = G = \frac{\pi\sigma^2 a}{E} \qquad \text{..... (7)}$$

and the stress intensity factor K_1 is equal to $\sigma\sqrt{\pi a}$ and substituting into (7) one obtains

$$G = \frac{K_1^2}{E} \Rightarrow K_1 = \sqrt{GE} \qquad \text{.....(8)}$$

The above equation shows that under LEFM condition, the prediction for crack growth and fracture is the same for both the energy balance and the elastic stress field approach.

4.2 Buckling Theory

For simplicity of analysis, the fiber strands subjected to the axial load were modeled as miniature columns. Using the buckling of column of strength of materials studies, one can determine the critical load acting on the fiber strand.

The critical load can be obtained by considering the behaviour of an ideal column, which assumed initially to be perfectly straight and compressed by a centrally applied load. The column is assumed to be perfectly elastic and when a load *P* is applied, will remain straight and undergoes only axial deflection. Therefore the moment at any cross section is given as

$$M = -P(\delta - y) \qquad \text{……. (9)}$$

and the differential equation is

$$EI\frac{d^2y}{dx^2} = -P(\delta - y) \qquad \text{……. (10)}$$

By integration, the solution of the above differential equation is

$$y = A\cos kx + B\sin kx + \delta \qquad \text{…… (11)}$$

Applying the boundary conditions, one can obtain the applied load expression as follows:

$$(2n-1)\frac{\pi}{2} = l\sqrt{\frac{P}{EI}} \qquad \text{…… (12)}$$

Since for $n > 1$ has no physical significance, therefore the smallest value of P will be when $n = 1$

$$P_{cr} = \frac{\pi^2 EI}{4l^2} \qquad \text{…… (13)}$$

The critical load P_{cr} is also know as the Euler load and is defined as the axial force which is sufficient to keep the bar in a slightly bent form.

5. Formulation of Equation

With reference to Figure 3 the bending moment at any cross section *mn* is

$$M = -P(\delta - y) \qquad \text{……. (9)}$$

and the differential equation is

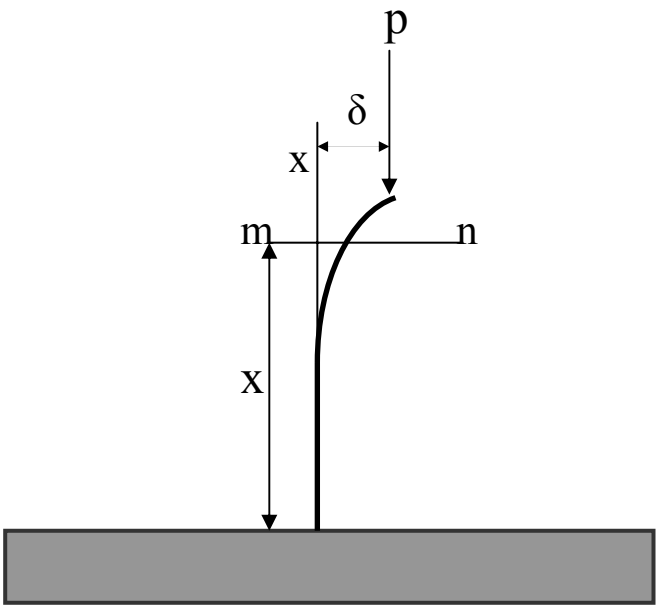

Figure 3: Diagram for formulation of equation

$$EI\frac{d^2y}{d^2x} = P(\delta - y) \qquad \text{..... (10)}$$

where *I* is the moment of inertia for buckling at the *xy* plane. Since

$$k^2 = \frac{P}{EI} \qquad \text{..... (14)}$$

one can write Equation (10) in the form of

$$\frac{d^2y}{d^2x} + k^2y = k^2\delta \qquad \text{..... (15)}$$

Since this is a non-homogenous 2nd order ordinary differential equation, the general solution of this equation is:

$$y = A\cos kx + B\sin kx + \delta \qquad \text{..... (16)}$$

To find the constants A and B, the two conditions at the fixed end of the bar were used. $y = \frac{dy}{dx} = 0$, at $x = 0$

These two conditions are fulfilled if

$$A = -\delta, \qquad B = 0$$

and then

$$y = \delta(1 - \cos kx) \qquad \text{……. (17)}$$

The condition at the upper end of the bar requires that

$$y = \delta \qquad \text{at } x = 1$$

which is satisfied if $\delta \cos kl = 0$

If $\delta = 0$, there is no deflection and hence no buckling, if $\cos kl = 0$, then one must have the relation $kl = (2n-1)\frac{\pi}{2}$ …… (18)

For the smallest P, n must be equal to 1, therefore

$$kl = l\sqrt{\frac{P}{EI}} = \frac{\pi}{2} \qquad \text{…….. (19)}$$

from which $P_{cr} = \frac{\pi^2 EI}{4l^2}$ ……. (13)

For a Mode I DCB specimen, as shown in Figure 4, the energy release rate is given as $G = \frac{12P^2a^2}{Eb^2h^3}$ ……..(20)

where *Pa* is the moment about O (Figure 4).

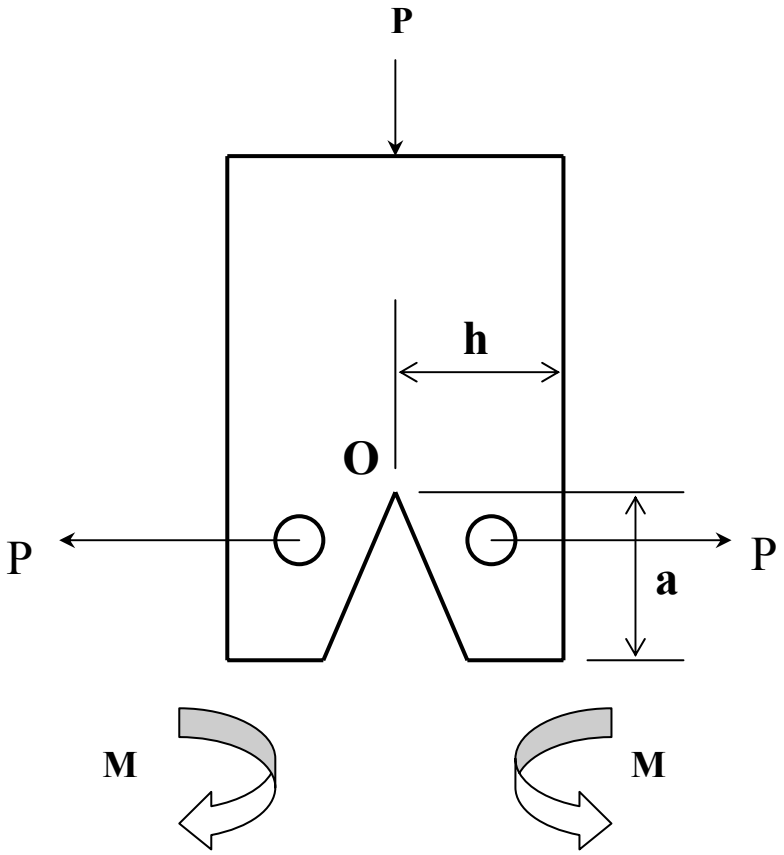

Figure 4: Mode I DCB Specimen

In order to compute the moment about O, consider the free body diagram in Figure 5.

The moment about O due to the force *P/2* is

$$M_1 = \frac{p}{2} a \sin\theta \qquad \text{..... (21)}$$

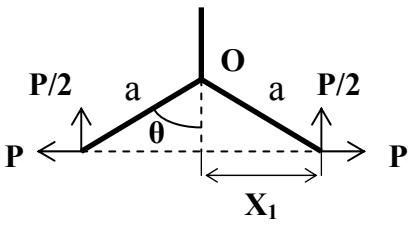

Figure 5: Free Body Diagram

The moment due to buckling on one arm of the specimen is

$$M_2 = -Px_1 \qquad \text{where } x_1 = a\cos\theta, \quad \text{and } P = P_{cr}$$

which gives $$M_2 = -\frac{\pi^2 EI}{4l^2} a\cos\theta \qquad \text{..... (22)}$$

Therefore total moment about O is $M_T = M_1 + M_2$

$$\mathrm{M_T} = \frac{P}{2} a\sin\theta - \frac{\pi^2 EI}{4l^2} a\cos\theta \qquad \text{..... (23)}$$

For Mode I energy release rate and re-arrange (13), one obtains

$$Pa = \sqrt{\frac{GEb^2h^3}{12}} \qquad \text{..... (24)}$$

Since *Pa* is the moment about O, therefore

$$Pa = M_T = \frac{P}{2} a\sin\theta - \frac{\pi^2 EI}{4l^2} a\cos\theta \qquad \text{..... (25)}$$

Substituting into (24)

$$\frac{p}{2} a\sin\theta - \frac{\pi^2 EI}{4l^2} a\cos\theta = \sqrt{\frac{GEb^2h^3}{12}} \qquad \text{..... (26)}$$

Divide both sides by *a sin θ*

$$\frac{p}{2} - \frac{\pi^2 EI}{4l^2}\sec\theta = \frac{1}{a\sin\theta}\sqrt{\frac{GEb^2h^3}{12}} \qquad \text{..... (27)}$$

Re-arrange the equation to obtain the force *P*

$$P = \frac{2}{a\sin\theta}\sqrt{\frac{GEb^2h^3}{12}} + \frac{\pi^2 EI}{2l^2}\sec\theta \qquad \text{..... (28)}$$

The moment of inertia I is given as $I = \frac{bh^3}{12}$

Substitute $I = \frac{bh^3}{12}$ into (28), one obtains

$$P = \frac{2}{a\sin\theta}\sqrt{\frac{GEb^2h^3}{12}} + \frac{\pi^2 Ebh^3}{24l^2}\sec\theta \qquad \text{..... (29)}$$

The mean crushing stress, σ_c, is given as

$$\sigma_c = \frac{P}{A} \qquad \text{..... (30)}$$

Therefore (29) becomes

$$\frac{P}{A} = \sigma_c = \frac{2}{a\sin\theta A}\sqrt{\frac{GEb^2h^3}{12}} + \frac{\pi^2 Ebh^3}{24l^2 A}\sec\theta \text{ ..... (31)}$$

where A is the area of one limb of the specimen and is equal to bh.

Substitute bh into (31) and re-arrange the terms, one obtains

$$\sigma_c = \frac{1}{a\sin\theta}\sqrt{\frac{GEh}{3}} + \frac{\pi^2 Eh^2}{24l^2}\sec\theta \qquad \text{..... (32)}$$

Since the above derivation is for one limb only, and for the whole specimen, the mean crushing stress should be doubled and

$$\sigma_c = \frac{2}{a\sin\theta}\sqrt{\frac{GEh}{3}} + \frac{\pi^2 Eh^2}{12l^2}\sec\theta \qquad \text{..... (33)}$$

Re-arrange (3) to obtain the energy release rate G

$$G = \frac{3(a\sin\theta)^2}{Eh}\left(\frac{\sigma_c}{2} - \frac{\pi^2 Eh^2 \sec\theta}{24l^2}\right)^2 \qquad \text{..... (34)}$$

6. Results and Discussions

For the convenience of comparison and calculations, the following assumptions were made,

a. A crack angle of 30º was used for all comparison.

b. A crack length of 5mm was used on all specimens.

c. The energy release rate of all the specimens values was obtained from the double cantilever beam (DCB) method.

The values used for all calculations were obtained from Hamada et al. and Hamada and Ramakrishna [5-7]. Table 1 summarizes the data used for calculations.

6.1 Calculation of σ_c using (33)

$$\sigma_c = \frac{2}{a\sin\theta}\sqrt{\frac{GEh}{3}} + \frac{\pi^2 Eh^2}{12l^2}\sec\theta \qquad \text{..... (33)}$$

was derived using LEFM (Linear Elastic Fracture Mechanics) and simple beam theory. One example of calculating the crushing stress (σ_c) of C/PEEK (0°) with crack length (a) equals to 5 mm is shown below:

$$\sigma_c = \frac{2}{a\sin\theta}\sqrt{\frac{GEh}{3}} + \frac{\pi^2 Eh^2}{12l^2}\sec\theta$$

Table 1: Data used for calculations

S/No	Materials used	E (GPa)	ρ (kg/m^3)	*l* (mm)	h (mm)	G (N/m)
1	C/PEEK (0˚)	131	1700	55	1.25	1560
2	C/PEEK (30˚)	65	1700	55	1.25	1560
3	C/EPOXY (45˚)	66	1500	55	1.25	120
4	GL/CLOTH-EPOXY #1	21.4	2020	55	1.25	1207
5	GL/CLOTH-EPOXY #2	20.9	2020	55	1.25	1196
6	GL/CLOTH-EPOXY #3	21.4	2020	55	1.25	979
7	GL/CLOTH-EPOXY #4	20	2020	55	1.25	1038
8	C/PEEK (B16)	134	1600	55	1.10	1750
9	C/PEEK (N16)	134	1600	55	1.045	1750
10	C/PEEK (N20)	134	1600	55	1.33	1750
11	C/PEEK (L116)	134	1600	55	1.07	1750

$$\sigma_c = \frac{2}{5x10^{-3}\sin 30°}\sqrt{\frac{1560\left(131x10^{9}\right)1.25x10^{-3}}{3} + \frac{3.14^2\left(131x10^{9}\right)\left(1.25x10^{-3}\right)^2}{12\left(55x10^{-3}\right)^2}}\frac{1}{\cos 30°}$$

= 297 x 10^6 Pascal.

Another example of calculating the crushing stress (σ_c) of C/PEEK (0°) with composite thickness (h) equals to 1 mm is shown below:

$$\sigma_c = \frac{2}{a\sin\theta}\sqrt{\frac{GEh}{3}} + \frac{\pi^2 Eh^2}{12l^2}\sec\theta$$

$$\sigma_c = \frac{2}{5x10^{-3}\sin 30°}\sqrt{\frac{1560\left(131x10^{9}\right)1.00x10^{-3}}{3} + \frac{3.14^2\left(131x10^{9}\right)\left(1.00x10^{-3}\right)^2}{12\left(55x10^{-3}\right)^2}}\frac{1}{\cos 30°}$$

= 250 x 10^6 Pascal.

The last example of calculating the crushing stress (σ_c) of C/PEEK (0°) with cracking opening (θ) equals to 5^o is shown below:

$$\sigma_c = \frac{2}{a\sin\theta}\sqrt{\frac{GEh}{3}} + \frac{\pi^2 Eh^2}{12l^2}\sec\theta$$

$$\sigma_c = \frac{2}{5x10^{-3}\sin 5°}\sqrt{\frac{1560\left(131x10^{9}\right)1.25x10^{-3}}{3} + \frac{3.14^2\left(131x10^{9}\right)\left(1.25x10^{-3}\right)^2}{12\left(55x10^{-3}\right)^2}}\frac{1}{\cos 5°}$$

= 1395 x 10^6 Pascal.

The calculated values were compared with values obtained from technical papers and research journals and were shown in Table 2. Comparisons were done on seven types of carbon fibres composites and 4 types of glass-cloth/epoxy.

Figure 6 shows that, for all composites considered, as the crack length (a) increases the crushing stress decreases exponentially. Figure 7 illustrates that, as the thickness (h) of the composite increases, the crushing stress increases exponentially. Figure 8 shows that, as the cracking opening (θ), increases from 0^o to 50^o, the crushing stress decreases exponentially; the crushing stress is at a minimum when $\theta = 50^o$. As the cracking opening increases, from 50^o to 80^o, the crushing stress increases slightly.

6.2Calculating Energy Release Rate (G) using (34)

$$G = \frac{3(a\sin\theta)^2}{Eh}\left(\frac{\sigma_c}{2} - \frac{\pi^2 Eh^2 \sec\theta}{24l^2}\right)^2 \qquad \text{.....(34)}$$

Calculated values of G using (34) are compared with values obtained from technical or research papers. Table 3 shows the comparison of these two values. One example of calculating the Energy Release Rate (G) of C/PEEK (0°) with crack length (a) equals to 5 mm is shown below:

$$G = \frac{3(a\sin\theta)^2}{Eh}\left(\frac{\sigma_c}{2} - \frac{\pi^2 Eh^2 \sec\theta}{24l^2}\right)^2$$

$$G = \frac{3\left(5x10^{-3}\sin 30°\right)^2}{131x10^9\left(1.25x10^{-3}\right)}\left(\frac{297x10^6}{2} - \frac{3.14^2\left(131x10^9\right)\left(1.25x10^{-3}\right)^2\frac{1}{\cos 30°}}{24\left(55x10^{-3}\right)^2}\right)^2$$

= 1551 N/m.

Table 2: Comparison of Crushing Stresses

S/No	Materials Used	σ_c (from Refs) x 10^6	σ_c using (33) x 10^6	Percentage Error (%)
1	C/PEEK (0°)	283	297	4.95%
2	C/PEEK (30°)	190	196	3.16%
3	C/EPOXY (45°)	79	78	1.27%
4	GL/CLOTH-EPOXY #1	110	93	15.45%
5	GL/CLOTH-EPOXY #2	106	92	13.20%
6	GL/CLOTH-EPOXY #3	91	85	6.59%
7	GL/CLOTH-EPOXY #4	90	84	6.67%
8	C/PEEK (B16)	327	285	12.84%
9	C/PEEK (N16)	334	274	17.96%
10	C/PEEK (N20)	356	332	6.74%
11	C/PEEK (L116)	309	279	9.71%

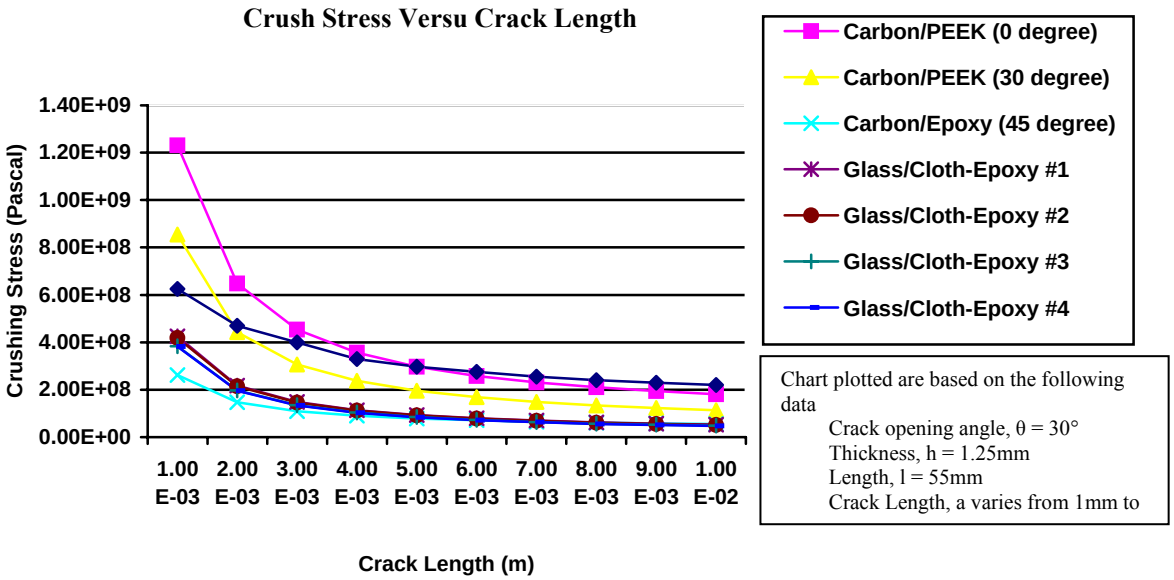

Figure 6: Crush versus crack length

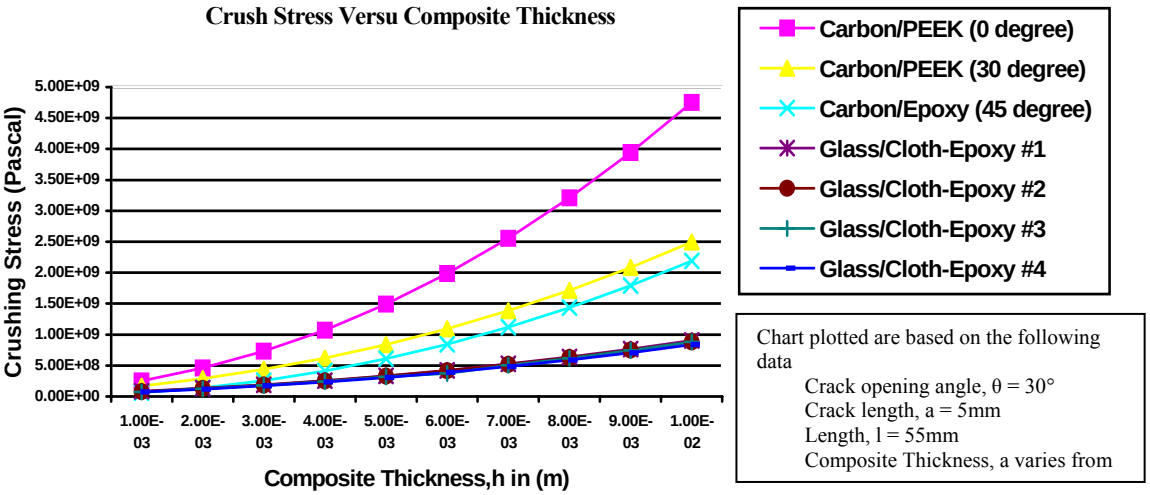

Figure 7: Crush versus crack length

For the crushing stress calculation, the comparison between the calculated results and experimental values seem reasonable. In the carbon fibre specimens, the largest percentage error was 17.96% and the least was 1.27%. Overall, the average error was about 8.09%.

For the glass-cloth/epoxy composites, the largest percentage error was 15.45% and the least was 6.59%. And average error of 10.48% was recorded for the glass-cloth/epoxy.

The energy release rate calculations were based on mean stress values obtained from experiments carried out by established sources. The average error obtained was about 0.49% and 6.63% for the carbon fibre specimens and glass-cloth/epoxy composites respectively; this error is even smaller compared to the crushing stress calculations.

From Figure 6, one can observe that carbon fibre specimens with a lower angle of fibre orientation agree quite well with the experimental data. As for the carbon fibre specimen of 45°, the error was quite substantial as compared with the experimental data. One likely cause of this large error is the effect of transverse ply cracking of the 45° specimen, which leads to localized fibre breakage.

Figure 7 shows the plot of crushing stress against the thickness, h. From the graph one can observe that the crushing stress or load increases as the thickness increases, this theoretical observation show a good agreement with experimental observation by Kim et al., which is shown in Figure 9 [17].

The term $\sqrt{GE}$ in (33) is the stress intensity factor of a material. The stress intensity factor of any material depends on the loading conditions and the mode of failure, i.e. Mode I, Mode II or mixed mode. Because of the nature of composite materials, the stress intensity factor can be quite difficult to obtain. Therefore the validity of stress intensity factors in composite materials is still an uncertainty and this may be the cause of the errors presented in the calculations.

Table 3: Comparison of *G* values

S/No	Materials Used	G (from Refs)	G (using Eqn 3-4)	Percentage Error (%)
1	C/PEEK (0°)	1560	1551	0.58%
2	C/PEEK (30°)	1560	1554	0.38%
3	C/EPOXY (45°)	120	118	1.67%
4	GL/CLOTH-EPOXY #1	1207	1193	1.16%
5	GL/CLOTH-EPOXY #2	1196	1485	24.16%
6	GL/CLOTH-EPOXY #3	979	973	0.61%
7	GL/CLOTH-EPOXY #4	1038	1032	0.59%
8	C/PEEK (B16)	1750	1746	0.23%
9	C/PEEK (N16)	1750	1744	0.34%
10	C/PEEK (N20)	1750	1750	0.00%
11	C/PEEK (L116)	1750	1746	0.23%

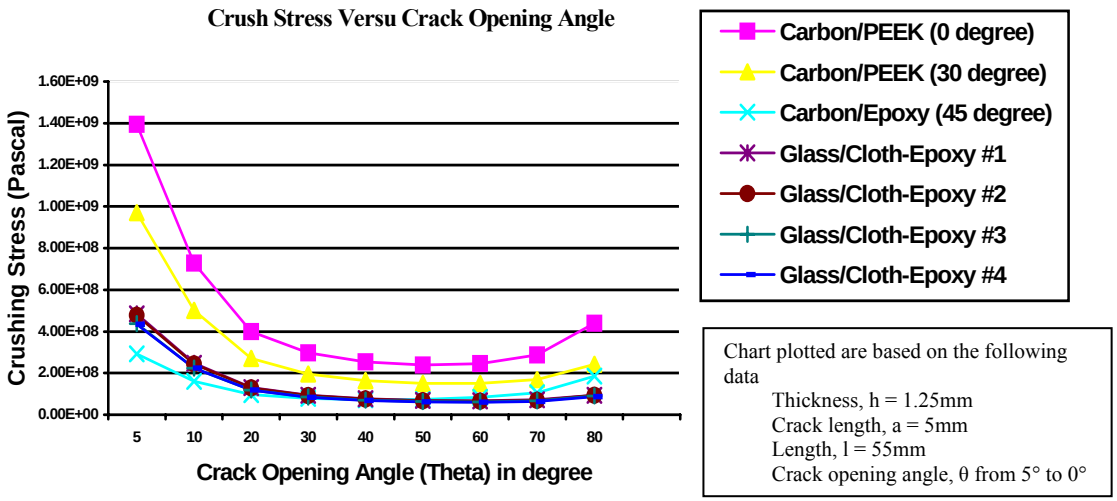

Figure 8: Crush stress versus opening angle

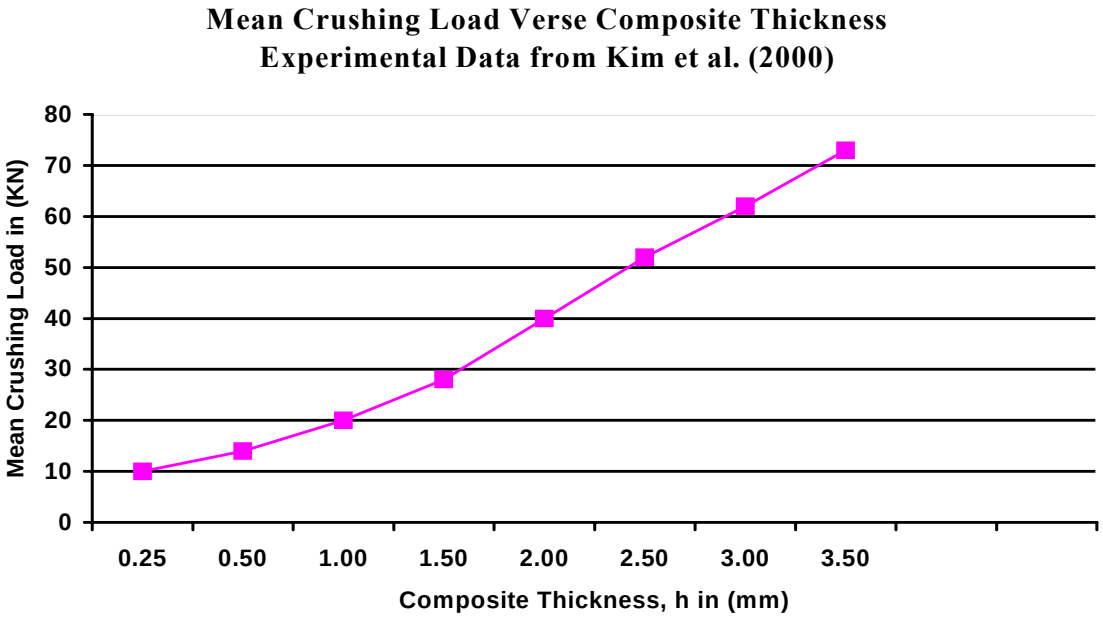

Figure 9: Mean crushing load verses composite thickness

There is also some limitation on the theories used since no material can withstand a stress, which is infinite in magnitude; the material in the vicinity of the crack tip is deformed in the plastic manner. As a result, the linear elastic fracture mechanics approach is valid for low nominal stress wherein the plastic zones are small relative to crack size and specimen boundaries and are totally confined in the elastic regions. The stress intensity factor provides a reasonably good approximation for stresses inside the unstable fracture region. But the expression for stress intensity factor is difference for loading conditions and modes of failure and the expression can be quite difficult to solve for same loading conditions.

In this project, Euler's buckling equation was used to derive the critical load (P_{Cr}) of the composite material. After obtaining the critical load, simple mechanics was used to find the moment acting on one limb of the model. Linear elastic fracture mechanics (LEFM) was used to derive the Mode I energy release rate (G). (33) and (34) are derived based on these two engineering concepts.

Certain assumptions were made when deriving the equations:

1) Linear elastics properties were assumed.

2) Thermal expansions between the piles were not considered.

3) Other modes of energy release rates were assumed to be negligible.

The calculated stresses and energy release rates were compared with experimental values obtained from research or technical papers. The results obtained can be summarized below:

- Results obtained from (33) and (34) agreed quite well with experimental values.
- The curves of (33) in Figure 7 agreed with established plot of the same nature.
- The Stress Intensity Factor, K_1 term in (33) played a apart in the error obtained because the validity of K_1 in composite is quite difficult to obtain due to the complex nature of the damage mechanisms.

7. Conclusion and Recommendations

The derived equation can predict or provide a reasonable stress prediction for most composite systems. The variables in the derived equation can be directly measured by experiments or can be obtained from handbooks or journals.

The mode of failure of the derived equation was based only on Mode I failure. It was therefore recommended that any future works or analysis on this project should include the other two modes of failures, i.e. Mode II and Mode III or the mixed mode [18].

Another area of interest for future development is the stress intensity factor (K_1).

The stress intensity factor for Mode I plane stress is given as

$$K = \sqrt{GE} \qquad \text{..... (8)}$$

and this term is present in (33)

Since there is no standard stress intensity factor solution, it might therefore be interesting to observe what might happen if different solutions of stress intensity factors were used.

References

1. Farley, G.L. and Jones, R.M. (1991). The Effect of Crushing Speed on the Energy Absorption Capability of Composite Tubes, Journal of Composite Materials, **26**: 1314-1329.

2. Farley, G.L. and Jones, R.M. (1992). Prediction of the Energy Absorption Capability of Composite Tubes, Journal of Composite Materials, **26**: 388-404.

3. Tao, W.H., Robertson, R.E. and Thornton, P.H. (1991). Effect of Materials Properties and Crush Conditions on the Crush Energy Absorption of Fibre Composite Rods, Composites Science and Technology, **47**: 405-418.

4. Hull D, (1991). A Unified Approach to Progressive Crushing of Fibre-Reinforced Composite Tubes, Composites Science and Technology, **40**: 377-421.

5. Hamada, H., Coppola, J.C. and Hull, D. (1992), Effect of Surface Treatment on Crushing Behavior of Glass Cloth/Epoxy Composite Tubes, Composites, **23**: 93-99.

6. Hamada, H., Coppola, J.C., Hull, D., Maekawa, Z. and Sato, H. (1992). Comparison of Energy Absorption of Carbon/Epoxy and Carbon/PEEK Composite Tubes, Composites, **23**: 245-252.

7. Hamada, H., Ramakrishna, S., and Satoh, H. (1995). Crushing Mechanism of Carbon Fibre/PEEK Composite Tubes, Composites, **26**: 749-755.

8. Gupta, N.K., Velmurugan, R. and Gupta, S.K. (1997). An Analysis of Axial Crushing of Composite Tubes, Journal of Composite Materials, **31**:1262-1286.

9. Dubey, D.D. and Vizzini, A.J. (1998). Energy Absorption of Composite Plates and Tubes, Journal of Composite Materials, **32**:158-176.

10. Wang, A.S.D. (1984). Fracture Mechanics of Sublaminate Cracks in Composite Laminates, Composite Technology Review, **6**: 45-62.

11. Crossman, F. and Wang, A.S.D. (1982). The Dependence of Transverse Cracking and Delamination on Ply Thickness in Graphite/Epoxy Laminates, ASTM STP 775.

12. O'Brien, T.K. (1982). Characterization of Delamination Onset and Growth in a Composite Laminate, *ASTM STP 775*, 140-167.

13. O'Brien, T.K., Johnston, N.J., Morris, D.H. and Simonds, R.A. (1982). A Simple Test for the Interlaminar Fracture Toughness of Composite", SAMPLE Journal, 8-15.

14. Sela, N. and Ishai, O. (1989). Interlaminar Fracture Toughness and Toughening of Laminated Composite Materials: A Review, Composite, **20**: 423-435.

15. Ramkumar, R.L. and Whitcomb, J.D. (1985). Characterization of Mode 1 and Mixed Mode Delamination Growth in T300/5208 Graphite/Epoxy, *ASTM STP 876*, 315-335.

16. Wilkins, D.J., Eisenmann, J.R., Chamin, R.A., Margolis, W.S. and Benson, R.A. (1982). Characterizing Delamination Growth in Graphite/Epoxy, *ASTM STP 775*, 168-183.

17. Kim, K.H., Shin, K.C. and Lee, J.J. (2000). Axial Crush and Energy Absorption Characteristics of Aluminum/GFRP Hybrid Square Tube, Key Engineering Materials, **183-187**: 1147-1152.

18. Callister, W.D. (2006). Materials science and engineering: an introduction, 7th Ed., John Wiley and Sons, Inc., 217-219.